# A Unified Framework for 3D Point Cloud Visual Grounding

Haojia Lin<sup>1\*</sup>, Yongdong Luo<sup>1\*</sup>, Xiawu Zheng<sup>2</sup>, Lijiang Li<sup>1</sup>, Fei Chao<sup>1</sup>, Taisong Jin<sup>1</sup>, Donghao Luo<sup>3</sup>, Chengjie Wang<sup>3</sup>, Yan Wang, Liujuan Cao<sup>1†</sup>

<sup>1</sup>Xiamen University, <sup>2</sup>Peng Cheng Laboratory, <sup>3</sup>Tencent Youtu Lab.

#### **Abstract**

3D point cloud visual grounding plays a critical role in 3D scene comprehension, encompassing 3D referring expression comprehension (3DREC) and segmentation (3DRES). We argue that 3DREC and 3DRES should be unified in one framework, which is also a natural progression in the community. To explain, 3DREC can help 3DRES locate the referent, while 3DRES can also facilitate 3DREC via more finegrained language-visual alignment. To achieve this, this paper takes the initiative step to integrate 3DREC and 3DRES into a unified framework, termed 3D Referring Transformer (3DRefTR). Its key idea is to build upon a mature 3DREC model and leverage ready query embeddings and visual tokens from the 3DREC model to construct a dedicated mask branch. Specially, we propose Superpoint Mask Branch, which serves a dual purpose: i) By leveraging the heterogeneous CPU-GPU parallelism, while the GPU is occupied generating visual tokens, the CPU concurrently produces superpoints, equivalently accomplishing the upsampling computation; ii) By harnessing on the inherent association between the superpoints and point cloud, it eliminates the heavy computational overhead on the high-resolution visual features for upsampling. This elegant design enables 3DRefTR to achieve both well-performing 3DRES and 3DREC capacities with only a 6% additional latency compared to the original 3DREC model. Empirical evaluations affirm the superiority of 3DRefTR. Specifically, on the ScanRefer dataset, 3DRefTR surpasses the state-of-the-art 3DRES method by 12.43% in mIoU and improves upon the SOTA 3DREC method by 0.6% Acc@0.25IoU. The code and models are available at https://github.com/Leon1207/3DRefTR.

## Introduction

The task of 3D Visual Grounding (3DVG) (Huang et al. 2021; Jain et al. 2022; Wu et al. 2023), has been gaining significant interest as a crucial 3D cross-modal challenge. The core goal of this task is to identify and locate an object within a 3D point cloud scene using a linguistic query, necessitating a comprehensive understanding of both the 3D visual information and the linguistic context.

Copyright © 2024, Association for the Advancement of Artificial Intelligence (www.aaai.org). All rights reserved.

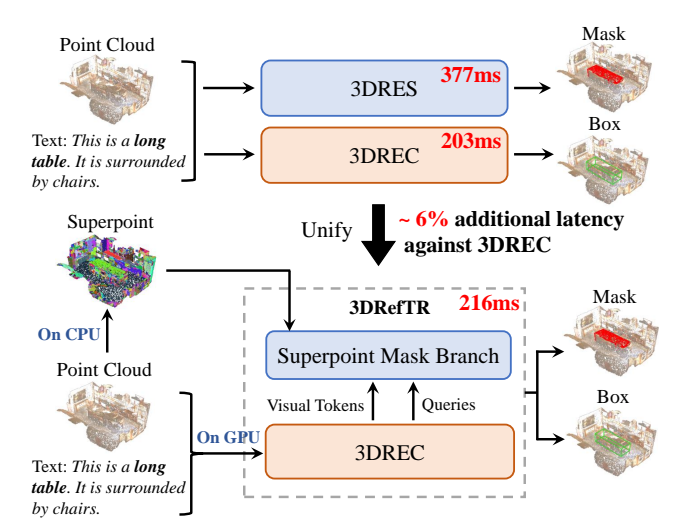


Figure 1: Utilizing two model specialized respectively for 3DREC and 3DRES, the computational cost for executing these two tasks is (203 + 377) milliseconds given the constraints of limited computation resource. In contrast, with Superpoint Mask Branch, 3DRefTR processes superpoints (On CPU) and visual tokens (On GPU) in parallel, unifying 3DREC and 3DRES with only a 6% increase in total latency compared to the original 3DREC model.

3DVG can be encountered two divergent yet interrelated tasks: 3D Referring Expression Comprehension (3DREC) (Huang et al. 2021; Jain et al. 2022) and 3D Referring Expression Segmentation (3DRES) (Huang et al. 2021). Various advances have been made in the domain of 3DREC, several contributions stand out: SAT (Yang et al. 2021) improves point cloud features extraction by 2D images assistance; BUTD (Jain et al. 2022) iteratively enhances object localization precision by incorporating Transformer's encoder-decoder architecture; EDA (Wu et al. 2023) refines object queries through explicit text decoupling and dense alignment. On the other hand, to the best of our knowledge, only one study, TGNN (Huang et al. 2021) paves its path to 3DRES, which remains this topic relatively untouched and necessitates further community exploration.

It is a natural idea to integrate 3DREC and 3DRES for

<sup>\*</sup>These authors contributed equally.

<sup>&</sup>lt;sup>†</sup>Communication Author.

mutual enhancement, as similar to the established practice of multi-task learning in 2D vision (Luo et al. 2020; Li and Sigal 2021; Zhu et al. 2022). The point-level supervision provided by 3DRES amplifies the capabilities of 3DREC, ensuring a more coherent language-vision alignment during multimodal training. On the other hand, 3DREC excels at localizing the referent object, addressing the limitations of RES in identifying the correct instance. Our ambition is to harmoniously fuse these tasks, proposing a unified methodology for 3DREC and 3DRES. Similar techniques have emerged in 2D visual grounding (Luo et al. 2020; Li and Sigal 2021; Zhu et al. 2022), offering insight into possible solutions for 3DVG. Yet, due to the intrinsic data characteristics of 3D point clouds, these techniques are challenging to transfer directly. For example, RefTR (Li and Sigal 2021) allocates specific backbone features for each query embedding and undergoes an upsampling decoder. However, due to the vast number of 3D point clouds, adopting this technique will result in an unfeasible computational overhead and memory consumption. Another method, SegTR (Zhu et al. 2022), aims to obtain masks by predicting polygons that encapsulate the masks, but three-dimensional spaces lack well-defined polygons to encapsulate 3D objects.

As shown in Fig. 1, the fundamental concept behind 3DRefTR entails an extension of a well-established 3DREC model, capitalizing on pre-existing query embeddings and visual tokens derived from the 3DREC model to construct a dedicated mask branch. This strategic approach effectively mitigates the additional computational cost that would arise from the integration of 3DRES capability. To further alleviate the computational burden associated with feature upsampling within the mask branch, we introduce the incorporation of superpoints (Landrieu and Simonovsky 2018). This introduces two primary advantages: i) Exploiting the inherent associations between the superpoints and point cloud to eliminate the intensive computation on high-resolution visual features during the upsampling process; ii) Leveraging heterogeneous CPU-GPU parallelism enables simultaneous CPU-driven superpoint generation while the GPU focuses on generating visual tokens, equivalently achieving the upsampling process. With the integration of the superpoint mask branch, 3DRefTR seamlessly unifies the capabilities of 3DREC and 3DRES with only a 6% addition latency against the original 3DREC model. Furthermore, the synergistic effect of unifying these two closely related tasks within a single model leads to mutual enhancement.

To sum up, the main contributions of this paper are as follows:

- Unified Framework for 3D Visual Grounding: We introduce the 3D Referring Transformer (3DRefTR), a pioneering framework that concurrently addresses both 3DREC and 3DRES tasks. Extensive experiments demonstrate that within our architecture, both tasks mutually enhance each other.
- Efficient Superpoint Mask Branch: Incorporating the superpoint mask branch into the 3DREC model, 3DRefTR delivers enhanced 3DRES and 3DREC capabilities with just a 6% latency increase compared to the

- original 3DREC model.
- Superior performance on the benchmarks: Empirical results on the ScanRefer dataset show that 3DRefTR outperforms the leading 3DRES method by a margin of 12.43% in mIoU and exceeds the state-of-the-art 3DREC method by 0.6% in Acc@0.25IoU.

## **Related Work**

### **3D Visual Grouding**

3D Visual Grounding (3DVG) aims to identify the targeted object in a 3D scene based on linguistic cues. Broadly, 3DVG encompasses two pivotal tasks: 3DREC and 3DRES. Within the 3DREC realm, most recent works (Zhao et al. 2021; Yang et al. 2021; Wu et al. 2023) adopt a two-stage pipeline. Initially, they harness ground truth or a 3D object detector (Jiang et al. 2020; Liu et al. 2021) to produce the object proposals. Subsequently, these methods use text and 3D encoder (Liu et al. 2019; Qi et al. 2017) to extract features and then ground the target one after the feature fusion. For instance, InstanceRefer (Yuan et al. 2021) ingeniously construes the task as instance-matching, while LanguageRefer (Roh et al. 2022) transforms it into a linguistic modeling task by replacing the 3D features with predicted object labels. BUTD (Jain et al. 2022) iteratively enhances object localization precision by incorporating Transformer's encoder-decoder architecture(Jain et al. 2022). 3D-SPS (Luo et al. 2022) first proposes a single-stage network, conceiving 3DVG as a keypoint selection problem. In contrast, the domain of 3DRES remains relatively untouched, with TGNN (Huang et al. 2021) being the solitary pioneer. This work hinges on an instance segmentation model, utilizing textguided Graph Neural Networks to identify the text-referred instance center.

A clear gap in current research is the lack of studies that tackle both 3DREC and 3DRES together. Our study aims to fill this gap by combining these two tasks into one unified framework, which not only simplifies deployment but also allows the tasks to benefit from each other.

#### 3D Detection and Segmentation

3D detection and segmentation algorithms stand as the cornerstone for 3DVG. Their significance in advancing 3DVG methods manifests primarily in two aspects. First, these detection algorithms directly provide object proposals for 2stage 3DVG methodologies as a part of the pipeline. Second, recent state-of-the-art 3DVG approaches, such as BUTD and EDA (Jain et al. 2022; Wu et al. 2023), have incorporated the query selection modules from Groupfree (Liu et al. 2021), indicating a converging trend of these technologies. Parallel to the latest 3DREC models like (Jain et al. 2022; Wu et al. 2023), contemporary 3D instance segmentation models, namely SPformer (Sun et al. 2023) and mask3D (Schult et al. 2023), also adopt the DETR-based architecture (Carion et al. 2020). However, due to the adoption of parametric query embeddings in these methods, their localization capabilities are inferior compared to the detectors that utilize feature-based query embeddings (Liu et al. 2021). In this context, our strategy in this paper is to leverage the precise

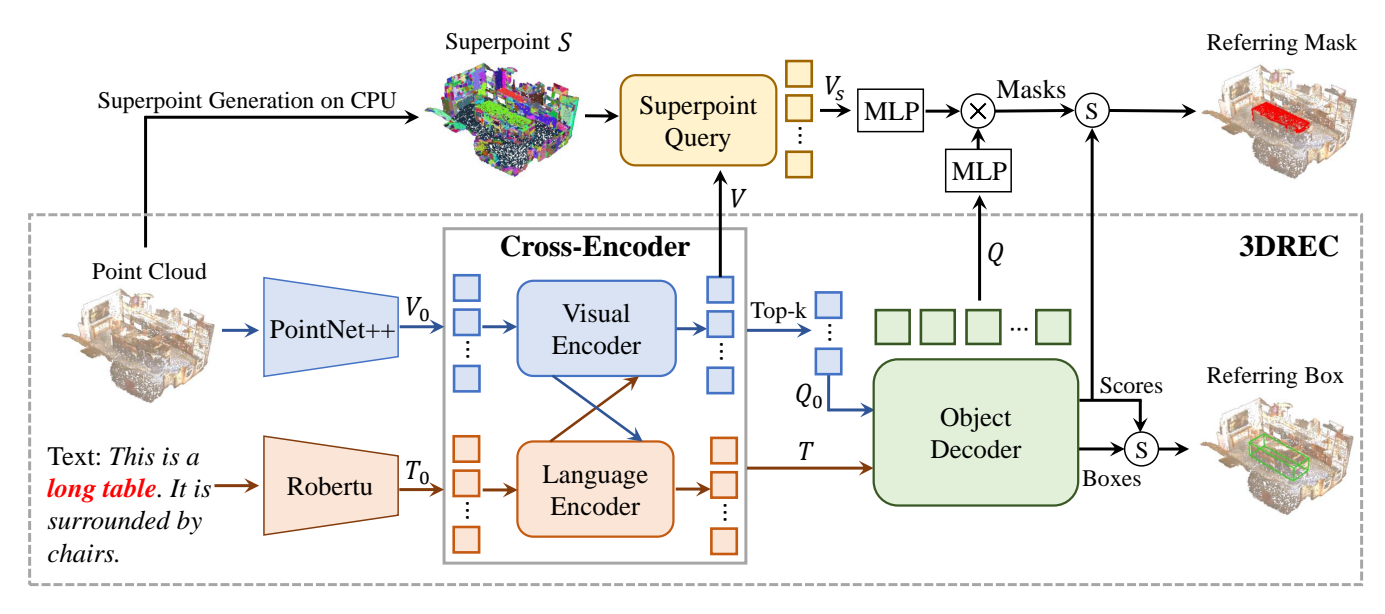


Figure 2: The framework of 3DRefTR builds upon a mature 3DREC model (enclosed by the gray dashed line) with a SuperPoint Mask Branch. For 3DRES, after obtaining the superpoint S and visual tokens V of each scene in parallel, S is used as the key to retrieve the corresponding nearest-neighbor features  $V_s$  from V by ball query.  $V_s$  and query embeddings Q are multiplied after MLP projection to obtain the candidate masks, which are then filtered by scores to obtain the referring mask.

localization capacity of the query embeddings in 3DREC. This approach not only mitigates the overhead introduced by incorporating 3DRES but also ensures the 3DREC capability remains uncompromised.

## Method

The key idea of 3DRefTR is to harness the ready localization capability of 3DREC model to develop the 3DRES potentials, subsequently utilizing the point-level supervisory signals of 3DRES to augment 3DREC performance. In this paper, we build 3DRefTR upon EDA (Wu et al. 2023) due to its superior performance for 3DREC. In the ensuing subsections, our 3DRefTR model appends an additional branch, explicitly for mask prediction. For a more comprehensive grasp of 3DRefTR, we start by briefly reviewing the EDA.

## **Preliminaries: 3DREC Model**

As shown in Fig. 2, the 3DREC model (enclosed by the gray dashed) is a typical DETR-like (Carion et al. 2020) model, which is composed of a backbone, a cross-encoder, and an object decoder.

**Visual and Textual Backbone.** PointNet++ (Qi et al. 2017) produces the visual tokens  $V_0 \in \mathbb{R}^{n \times d}$  from the input point cloud  $P \in \mathbb{R}^{N \times 3}$ , while Roberta-base (Liu et al. 2019) processes referential text for text tokens  $T_0 \in \mathbb{R}^{l \times d}$ , where n denotes the number of visual token, l denotes the number of text token, N denotes the point cloud size, and d is the feature dimension.

**Cross-Encoder.** The visual tokens  $V_0$  and text tokens  $T_0$  enter a dual-pathway cross-encoder alternatively stacking with self-attention, cross-attention, and FFN layers, producing thoroughly fused features  $V \in \mathbb{R}^{n \times d}$  and  $T \in \mathbb{R}^{l \times d}$ . The

output visual tokens  $V \in \mathbb{R}^{n \times d}$  is input to the KPS module proposed by (Liu et al. 2021). The top-k object queries  $Q_0 \in \mathbb{R}^{k \times d}$  are chosen and then fed into the object decoder and the query scoring branch.

**Object Decoder.** The top-k object queries  $Q_0$  and the text tokens T enter the object decoder which consists of stacked Transformer decoder layers, producing the final query embeddings  $Q \in \mathbb{R}^{k \times d}$ . On top of these object query embeddings Q, the decoder has two branches respectively for box regression and box-text alignment. The box branch dynamically updates boxes  $B \in \mathbb{R}^{k \times 6}$  and provides position embeddings for query embeddings in each Transformer decoder layer. The alignment branch output the referring scores  $s \in \mathbb{R}^k$  for the query embeddings to determine which query best matches the referent. Given the existing box and alignment branches, the query embeddings Q in 3DREC model exhibit inherent localization abilities. The pivot is to harness these embeddings to construct the mask branch to unlock the segmentation potential of the model.

## **Naive Mask Branch**

Inspired by MaskDINO (Li et al. 2023), the most straightforward approach to construct the mask branch is to first pass the visual tokens through an upsampling decoder  $U(\cdot)$ , obtaining the original-resolution visual tokens  $V_0 \in \mathbb{R}^{N \times d}$ . Subsequently, by multiplying it with the ready query embeddings Q in the 3DREC model, we derive a mask prediction  $M_0 \in [0,1]^{N \times k}$  with the original resolution. Employing this mask branch construction strategy, we can realize a unified model proficient in both 3DREC and 3DRES tasks, which is named 3DRefTR-HR.

However, a challenge arises due to the vast original point cloud size N, which often exceeds 50,000 in datasets like

Method	FLOPs (G)	Component Time (ms)	Total (ms)
EDA	9.82	=	203
3DRefTR-HR	24.38	-	405
3DRefTR-SP	10.68	Before S (CPU):180 Before V (GPU):172 After V (GPU):36	216

Table 1: Efficiency analysis for 3DRefTR-SP.

ScanNet. This addition of the mask branch subsequently inflates the computational demand for the entire model by approximately 140% (As shown in Tab. 1). Such a surge in computation, when taken in the broader context of real-time applications and resource constraints, renders this naive approach suboptimal. It thus encourages us to search for a more efficient mask branch design.

## **Superpoint Mask Branch**

Moving forward, our objective is to develop an approach that strikes a balance between performance and efficiency for the added mask branch in our 3DRefTR. Inspired by works (Landrieu and Simonovsky 2018), we turn to superpoints as a bridge connecting low-resolution features with the high-resolution point cloud, paving the way for a more efficient upsampling technique.

Superpoint Generation on CPU. For the input point cloud  $P \in \mathbb{R}^{N \times 3}$ , superpoints  $S \in \mathbb{R}^{m \times 3}$  define geometrically homogeneous neighborhoods of its local points, and are usually computed by over-segmenting P using graph partition<sup>1</sup>. In another word, there is a mapping  $\phi: P \in \mathbb{R}^{N \times 3} \to S \in \mathbb{R}^{m \times 3}$  between the superpoints S and the original point cloud P. Therefore, the prediction of the original mask  $M_0$  can be reformulated as the prediction of the superpoint mask  $M_s$ . Because the  $\phi$  is equivalent to the upsampling function and the superpoint generation can be conducted on CPU, the computation of upsampling is shifted to precede the cross-encoder output, parrallelling with producing the visual tokens V.

**Superpoint Query.** The next step involves acquiring the visual embedding for each superpoint. To achieve this, we design a parameter-free superpoint query module. Given the output visual tokens V' from the cross-encoder and the superpoints S, we employ the ball query (Qi et al. 2017) to find the nearest neighbor tokens in coordinate space for each superpoint. Subsequent max-pooling is used for aggregation, producing the superpoint embeddings  $V_s \in \mathbb{R}^{m \times d}$ .

Superpoint Mask Prediction. Lastly, the generated superpoint embeddings  $V_s$  and the ready query embeddings Q from the 3DREC model are separately passed through a Multilayer Perceptron (MLP). Their respective outputs are then multiplied, resulting in the superpoint binary masks  $M_s \in [0,1]^{m \times k}$ . The original mask  $M_0$  can be easily acquired from  $M_s$  via the mapping  $\phi$ .

## **Highlights on Efficiency**

The essence of Superpoint Mask Branch is its dual-edge advantage: i) it eliminates the heavy computational overhead on the high-resolution visual features during upsampling; ii) by conducting upsampling computations prior to the cross-encoder output, the approach leverages heterogeneous CPU-GPU parallelism, achieving upsampling with minimal overhead

Compared with 3DRefTR-HR. As depicted in Tab. 1, the introduction of an upsampling decoder in 3DRefTR-HR inflates computational demands by 2.5 times compared to the original model and doubles the inference latency. In contrast, the FLOPs and latency of the 3DRefTR-SP model see only modest increments of 8% and 6% against the 3DREC model, respectively. Of paramount significance is that the Superpoint Mask Branch shifts the computational burden of upsampling (i.e., superpoint generation) to precede the cross-encoder output. As shown in Tab. 1, the model's latency from input to cross-encoder output V is 172 ms, roughly equivalent to the 180 ms consumed by superpoint S generation. Given that superpoint generation is executed on the CPU, it doesn't compete for computational resources with the main model components and can run in parallel.

Compared with SPformer (Sun et al. 2023) and SSTNet (Liang et al. 2021). It is essential to highlight the distinctions of superpoint usage between our approach, SPformer, and SSTNet. These methods employ superpoints as an integral part of their backbone for feature aggregation. As a result, the generation of superpoints inevitably consumes a significant portion of the model's forward-pass time. However, our approach contrasts this by leveraging the heterogeneous computing of CPU and GPU. During the timegap where our mask branch awaits the output visual tokens from the cross-encoder, we allocate the superpoint generation task. This procedure effectively exploits CPU-GPU parallelism, facilitating the addition of 3DRES capabilities to the 3DREC model with almost negligible additional cost.

In summing up, the pivotal insight of this paper is the maximal reuse of a well-performing 3DREC model to seamlessly and efficiently integrate 3DRES capabilities into a unified framework. The design of our proposed Superpoint Mask Branch seamlessly aligns with this fundamental principle.

#### **Multi-task Training**

This subsection illustrates the loss functions and the joint training scheme for 3DRefTR.

**Loss Function.** For the 3DREC task, we follow the training scheme of EDA (Wu et al. 2023), which adopts five loss functions for each layer of the object decoder: box center coordinate prediction with a smooth- $L_1$  loss  $\mathcal{L}_{\text{coord}}$ , box size prediction with a smooth- $L_1$  loss  $\mathcal{L}_{\text{size}}$ , GIoU loss (Rezatofighi et al. 2019)  $\mathcal{L}_{\text{giou}}$ , the semantic alignment loss  $\mathcal{L}_{\text{sem}}$ , and the position alignment loss  $\mathcal{L}_{\text{pos}}$ . The loss of i-th decoder layer is the combination of these 5 loss terms by weighted summation:

$$\mathcal{L}_{\text{dec}}^{(l)} = \beta_1 \mathcal{L}_{\text{coord}}^{(l)} + \beta_2 \mathcal{L}_{\text{size}}^{(l)} + \beta_3 \mathcal{L}_{\text{giou}}^{(l)} + \beta_4 \mathcal{L}_{\text{sem}}^{(l)} + \beta_5 \mathcal{L}_{\text{pos}}^{(l)} \,.$$

<sup>&</sup>lt;sup>1</sup>We utilize superpoint generation codes of SPFormer for this purpose: https://github.com/sunjiahao1999/SPFormer.

Method	Unique(19%)		Multiple(81%)		Overal		m I a I I
	0.25	0.5	0.25	0.5	0.25	0.5	mIoU
TGNN (Huang et al. 2021)	-	-	-	-	37.50	31.40	27.80
3DRESTR	78.99	54.19	40.19	22.07	45.98	26.87	28.74
EDA-box2mask (Wu et al. 2023)	84.71	56.94	49.98	37.03	55.16	39.99	35.03
3DRefTR-HR (ours)	89.64	77.03	52.31	43.71	57.88	48.69	41.24
3DRefTR-SP (ours)	87.88	69.77	51.61	41.91	57.02	46.07	40.76
single-stage							
EDA-box2mask (Wu et al. 2023)	84.50	55.46	49.02	36.38	54.31	39.23	34.67
3DRefTR-HR (ours)	89.71	76.11	51.45	43.07	57.16	48.00	40.75
3DRefTR-SP (ours)	86.75	69.56	50.67	41.18	56.06	45.36	40.23

Table 2: The 3D referring expression segmentation results on ScanRefer. Compared to the two-stage methods, TGNN (Huang et al. 2021) and two other established baselines, the signle-stage 3DRefTR-SP supasses with a margin of 12.43%, 11.49%, and 5.2% in mIoU, respectively.

The losses on all decoder layers are averaged to form the total 3DREC loss:

$$\mathcal{L}_{
m rec} = rac{1}{L} \sum_{l=1}^{L} \mathcal{L}_{
m dec}^{(l)}$$
 .

For the 3DRES task, we follow RefTR (Li and Sigal 2021) and apply the focal loss (Lin et al. 2017)  $\mathcal{L}_{\text{focal}}$  and the dice loss (Milletari, Navab, and Ahmadi 2016)  $\mathcal{L}_{\text{dice}}$  on the top of the last layer of the object decoder. Together with the KPS loss (Liu et al. 2021)  $\mathcal{L}_{\text{kps}}$  for the query selection, the final loss for 3DRefTR is as follows:

$$\mathcal{L} = \alpha_1 \mathcal{L}_{rec} + \alpha_2 \mathcal{L}_{focal} + \alpha_3 \mathcal{L}_{dice} + \alpha_4 \mathcal{L}_{kps}.$$

**Joint Training.** For efficient convergence, we initiate the joint training process by loading pre-trained weights from the 3DREC model. Subsequently, the training unfolds with a learning rate set at 0.01 times the standard rate for the 3DREC component, while the superpoint mask branch is trained using the standard learning rate. This training scheme has demonstrated its efficacy in maintaining a favorable equilibrium between the performance of 3DREC and 3DRES. A thorough analysis of the impact of this training scheme will be shown in the section of the Ablation Study.

## Inference

During inference, given an input point cloud and a referring text, 3DRefTR outputs the superpoint masks  $M_s \in [0,1]^{m \times k}$  and the object boxes  $B \in \mathbb{R}^{k \times 6}$ . Subsequently, the referent mask and box will be selected according to the referring scores  $s \in \mathbb{R}^k$ .

## **Experiments**

## **DataSets**

We assess our approach on 3D referring datasets, including ScanRefer (Chen and Chang 2020) and ReferIt3D (Achlioptas et al. 2020). These datasets derive from ScanNetv2 (Dai et al. 2017), featuring 1,513 detailed 3D indoor scene reconstructions. All datasets adhere to the official ScanNet splits.

**ScanRefer** offers 51,583 descriptions, averaging 13.81 objects and 64.48 descriptions per scene. Its evaluation metric is Acc@IoU, measuring the proportion of descriptions

where the predicted box and ground truth overlap with an IoU greater than 0.25 and 0.5. Descriptions are categorized into "unique" if the object is the sole representative of its class in the scene, or "multiple" otherwise.

**ReferIt3D** includes two subsets: Sr3D and Nr3D. Sr3D encompasses 83,572 template-generated expressions, while Nr3D houses 41,503 human-generated expressions. Instead of presenting the full scene, this dataset offers segmented point clouds for individual objects. The primary evaluation metric for ReferIt3D is accuracy, gauging if the model aptly identifies the target object.

## **Implementation Details**

Our model is trained with the AdamW optimizer and a batch size of 12 on four NVIDIA V100 GPUs for 100 epochs. We freeze the text backbone Robeta-base following the settings in (Wu et al. 2023), while the rest of the network is trainable. The initial learning rates of the PointNet++ backbone and the rest of the model are empirically set to 2e-3 and 2e-4, respectively. We apply learning rate decay at epochs 50 and 75 with a rate of 0.1. For all the datasets, we use xyz coordinates and RGB values as the input, and the number of visual tokens V and query embeddings Q are empirically set to 1024 and 256, respectively. The sample number and radius of the ball query are set to 2 and 0.2, respectively. The number of decoder layers L is set to 6. The balancing factors are set default as  $\alpha_1 = 1.0 / (L + 1)$ ,  $\alpha_2 = 10.0$ ,  $\alpha_3 =$ 2.0,  $\alpha_4 = 8.0$ ,  $\beta_1 = 5.0$ ,  $\beta_2 = 1.0$ ,  $\beta_3 = 1.0$ ,  $\beta_4 = 0.5$  and  $\beta_5$ = 0.5 for the ScanRefer dataset. For the Nr3D/Sr3D dataset,  $\beta_4$  and  $\beta_5$  are adjusted to be 1.0 and 1.0, respectively.

## **Quantitative Comparison**

In this subsection, we perform a qualitative comparison on ScanRefer (Chen and Chang 2020) and Referit3D (Achlioptas et al. 2020).

**3DRES.** To the best of our knowledge, TGNN (Huang et al. 2021) is the only relevant study for the 3DRES task. To ensure a more fair comparison, we established two baseline methods, namely 3DRESTR and EDA-box2mask, based on the state-of-the-art 3DREC approach EDA (Wu et al. 2023). The 3DRESTR shares a nearly identical network structure with EDA, with the sole distinction being the substitution

Method	Unique(19%)		Multiple(81%)		Overal		
Wiethod	0.25	0.5	0.25	0.5	0.25	0.5	
ScanRefer (Chen and Chang 2020)	67.64	49.19	32.06	21.26	38.97	26.10	
TGNN (Huang et al. 2021)	68.61	56.80	29.84	23.18	37.37	29.70	
3DJCG (Cai et al. 2022)	78.75	61.30	40.13	30.08	47.62	36.14	
D3Net (Chen et al. 2021)	-	70.35	-	30.50	-	37.87	
BUTD (Jain et al. 2022)	82.88	64.98	44.73	33.97	50.42	38.60	
EDA (Wu et al. 2023)	85.69	70.19	49.60	38.39	54.99	43.13	
3DRefTR-HR (ours)	85.98	70.89	49.62	38.30	55.04	43.16	
3DRefTR-SP (ours)	86.12	71.04	50.07	38.65	55.45	43.48	
single-stage							
3DSPS (Luo et al. 2022)	84.12	66.72	40.32	29.82	48.82	36.98	
BUTD (Jain et al. 2022)	81.47	61.24	44.20	32.81	49.76	37.05	
EDA (Wu et al. 2023)	86.40	69.42	48.11	36.82	53.83	41.70	
3DRefTR-HR (ours)	86.75	67.94	48.73	37.79	54.40	42.29	
3DRefTR-SP (ours)	86.40	68.01	48.82	37.83	54.43	42.33	

Table 3: The 3D referring expression comprehension results on ScanRefer in terms of Acc@0.25IoU and Acc@0.5IoU. Our 3DRefTR surpasses existing state-of-the-art works in both two-stage and single-stage setting with a significant margin.

Method	Sr3D	Nr3D
ReferIt3D (Achlioptas et al. 2020)	39.8	35.6
TGNN (Huang et al. 2021)	45.0	37.3
3DSPS (Luo et al. 2022)	62.6	51.5
BUTD (Jain et al. 2022)	65.6	49.1
EDA (Wu et al. 2023)	68.1	52.1
3DRefTR-SP (ours)	68.5	52.6

Table 4: The 3DREC performance on SR3D/NR3D datasets by Acc@0.25IoU as the metric.

of the box regression branch in the object decoder with a mask branch. Meanwhile, the EDA-box2mask converts the box output from the EDA model into a mask, i.e., filtering points in the 3D scene using the outputted 3D bounding box. As reflected in Tab. 2, our proposed 3DRefTR significantly outperforms these baseline methods across both two-stage and single-stage settings. Specifically, in terms of mIoU, the two-stage 3DRefTR-SP surpasses TGNN, 3DRESTR, and EDA-box2mask by margins of 12.96%, 12.02%, and 5.73% respectively. The performance of single-stage 3DRefTR-SP is comparably impressive. Notably, although 3DRefTR-HR showcases superior segmentation performance over 3DRefTR-SP, the marginal gains do not seem compelling when weighed against its considerably higher computational demands.

**3DREC.** To evaluate the 3DREC performance, we compare 3DRefTR with several existing 3DREC works on Scan-Refer and ReferIt3D, involving the state-of-the-art DETR-like methods EDA (Wu et al. 2023) and BUTD (Jain et al. 2022), the single-stage model 3D-SPS (Luo et al. 2022), the segmentation-based two-stage method TGNN (transform the predicted mask into the box) (Huang et al. 2021), among others. As evidenced in Tab. 3 and Tab. 4, 3DRefTR consistently exhibits superior performance over these prevailing methods in both two-stage and single-stage settings. This evidence strongly suggests that the newly incorporated mask prediction branch has indeed augmented the perfor-

mance of the 3DREC task. The commendable results can be largely attributed to the well-constructed design of our unified 3DVG framework.

## **Ablation Study**

In this subsection, we delve into the influence of varying configurations on the performance of 3DRefTr. Broadly speaking, due to the streamlined and efficient nature of our method, there is minimal parameter tuning required to achieve optimal performance. The experiments in this subsection are conducted on Scanrefer and metrics adopted for 3DREC and 3DRES performance are Acc@0.25IoU and mIoU, repectively.

**Auxiliary Segmentation Head.** Every Transformer layer in the object decoder is connected to a box branch. This observation led us to consider the addition of a mask prediction head after each layer of the decoder, serving as an auxiliary head. However, the results from Table 5 indicate that the presence or absence of an auxiliary head has a negligible impact on the overall performance. Consequently, in practical implementations, we opt for a single mask head, primarily considering the training costs.

Joint Training Scheme. We explore the impacts of different joint training schemes on task performance. Five training schemes were investigated for 3DRefTR: 1) jointly training from scratch, 2) loading the pretrained 3DRES model and jointly training 3DRES and 3DREC, 3) loading the pretrained 3DREC model and jointly training 3DRES and 3DREC, 4) freezing the pretrained 3DREC component and training the Superpoint Mask Branch alone, 5) loading the pretrained 3DREC model and jointly training 3DRES and 3DREC with different learning rates (2e-4 and 2e-6). As displayed in Tab. 6, The 1st, 2nd, and 3rd scheme cause a suboptimal 3DREC performance and the 4rd scheme showcases the best performance for the 3DREC task, inspiring us to apply a smaller learning rate on the 3DREC components (the 5th scheme) for better trade-off. The 5th scheme with different learning rates for 3DRES and 3DREC demonstrates the most optimal trade-off.

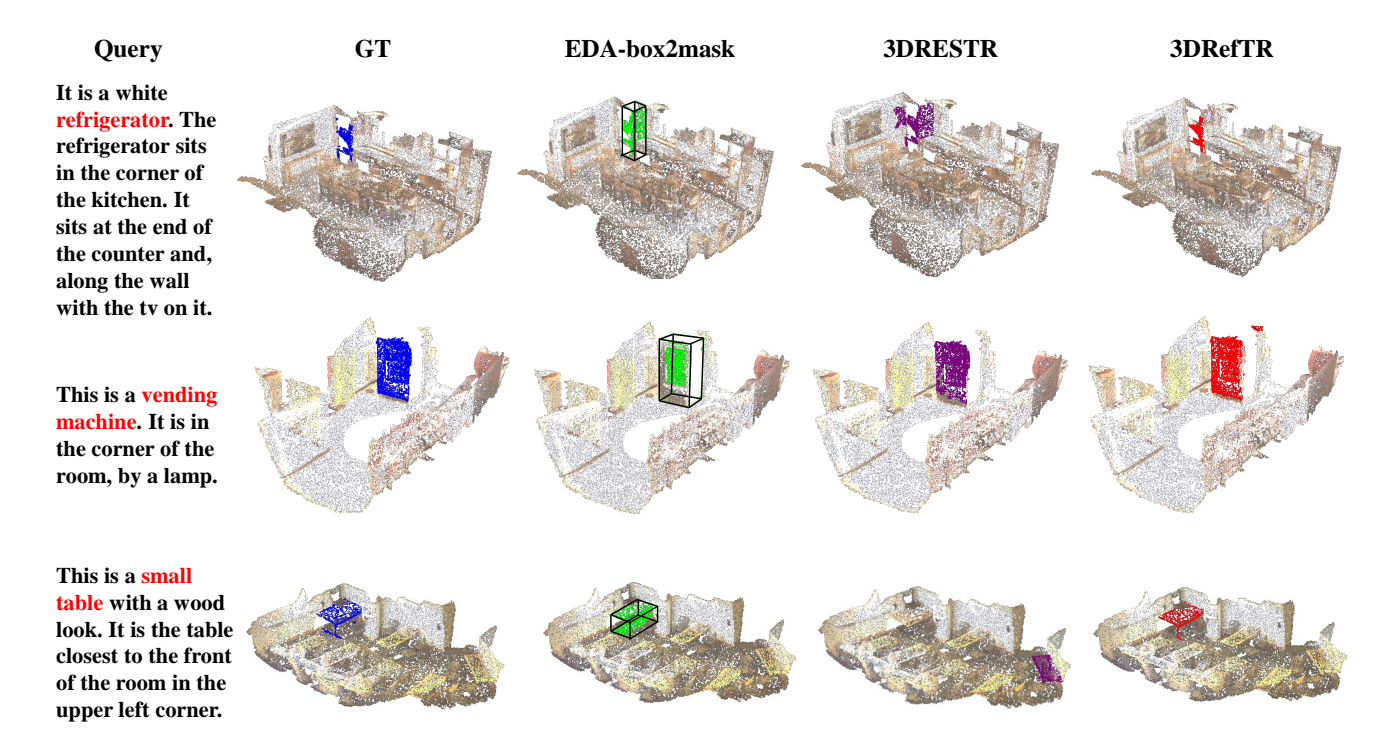


Figure 3: Visualization of the 3D refering expression segmentation results. EDA-box2mask has difficulties with mask boundaries. 3DRESTR exhibits weak localization. However, 3DRefTR-SP excels in both localization and mask refinement.

## Qualitative comparison

The visualization of the results for 3D Referring Expression Segmentation is presented in Fig. 3. EDA-box2mask displays commendable localization capabilities. However, the points filtered out by its box often encounter challenges in handling the mask boundaries. As a consequence, there are frequent instances of incomplete masks or residues from other objects. 3DRESTR, on the other hand, exhibits prowess in precisely managing mask boundaries. Nevertheless, its localization ability is found wanting, as evidenced in the third row, resulting in the lowest mIoU score. Contrastingly, our proposed 3DRefTR-SP excels in both precise localization and impeccable handling of mask boundaries.

## **Conclusions**

This work introduced the 3D Referring Transformer, 3DRefTR, an innovative approach that concurrently addresses the multi-task challenges of 3D referring expression comprehension and 3D referring expression segmentation. Through the strategic integration of a superpoint-based mask branch, the model not only advances the state-of-the-art in high-resolution segmentation but also achieves a refined alignment between linguistic and visual representations, further bolstering the performance of 3DREC. A significant innovation in our framework is the exploitation of heterogeneous CPU-GPU parallelism. By leveraging this parallelism, 3DRefTR efficiently harnesses the capabilities of both processing units, allowing the CPU to generate superpoints concurrently while the GPU produces visual to-

Auxiliary Head	w/o	w/
3DREC	55.45	55.31
3DRES	40.76	40.57

Table 5: Performance on Scanrefer affected by the presence or absence of the auxiliary segmentation heads. The metrics for 3DREC and 3DRES are Acc@0.25IoU and mIoU.

Training Scheme	3DRES	3DREC
Scratch Training	41.39	54.61
3DRES then Joint	41.21	54.70
3DREC then Joint	40.65	54.02
3DREC frozen	40.20	54.99
3DREC then Joint (Two lr)	40.76	55.45

Table 6: Performance on Scanrefer affected by different training schemes. 'Two Ir' means jointly training 3DRES and 3DREC components with different learning rates.

kens. This parallel processing mitigates the computational challenges traditionally associated with high-resolution visual tasks, ensuring efficient and scalable model operation. To conclude, the 3DRefTR framework marks a step forward in 3D visual grounding. Its ability to harmoniously unify 3DREC and 3DRES tasks, backed by computational efficiency and good performance, underscores its potential in advancing the field of 3D scene comprehension.

## References

- Achlioptas, P.; Abdelreheem, A.; Xia, F.; Elhoseiny, M.; and Guibas, L. 2020. Referit3d: Neural listeners for fine-grained 3d object identification in real-world scenes. In *Computer Vision–ECCV 2020: 16th European Conference, Glasgow, UK, August 23–28, 2020, Proceedings, Part I 16*, 422–440. Springer.
- Cai, D.; Zhao, L.; Zhang, J.; Sheng, L.; and Xu, D. 2022. 3djcg: A unified framework for joint dense captioning and visual grounding on 3d point clouds. In *Proceedings of the IEEE Conference on Computer Vision and Pattern Recognition*, 16464–16473.
- Carion, N.; Massa, F.; Synnaeve, G.; Usunier, N.; Kirillov, A.; and Zagoruyko, S. 2020. End-to-end object detection with transformers. In *European conference on computer vision*, 213–229. Springer.
- Chen, D. Z.; and Chang, A. X. 2020. Scanrefer: 3d object localization in rgb-d scans using natural language. In *European conference on computer vision*, 202–221. Springer.
- Chen, D. Z.; Wu, Q.; Nießner, M.; and Chang, A. X. 2021. D3Net: a speaker-listener architecture for semi-supervised dense captioning and visual grounding in RGB-D scans.
- Dai, A.; Chang, A. X.; Savva, M.; Halber, M.; Funkhouser, T.; and Nießner, M. 2017. Scannet: Richly-annotated 3d reconstructions of indoor scenes. In *Proceedings of the IEEE conference on computer vision and pattern recognition*, 5828–5839.
- Huang, P.-H.; Lee, H.-H.; Chen, H.-T.; and Liu, T.-L. 2021. Text-guided graph neural networks for referring 3d instance segmentation. In *Proceedings of the AAAI Conference on Artificial Intelligence*, volume 35, 1610–1618.
- Jain, A.; Gkanatsios, N.; Mediratta, I.; and Fragkiadaki, K. 2022. Bottom up top down detection transformers for language grounding in images and point clouds. In *European Conference on Computer Vision*, 417–433. Springer.
- Jiang, L.; Zhao, H.; Shi, S.; Liu, S.; Fu, C.-W.; and Jia, J. 2020. Pointgroup: Dual-set point grouping for 3d instance segmentation. In *Proceedings of the IEEE conference on computer vision and Pattern recognition*, 4867–4876.
- Landrieu, L.; and Simonovsky, M. 2018. Large-scale point cloud semantic segmentation with superpoint graphs. In *Proceedings of the IEEE conference on computer vision and pattern recognition*, 4558–4567.
- Li, F.; Zhang, H.; Xu, H.; Liu, S.; Zhang, L.; Ni, L. M.; and Shum, H.-Y. 2023. Mask dino: Towards a unified transformer-based framework for object detection and segmentation. In *Proceedings of the IEEE Conference on Computer Vision and Pattern Recognition*, 3041–3050.
- Li, M.; and Sigal, L. 2021. Referring transformer: A one-step approach to multi-task visual grounding. *Advances in neural information processing systems*, 34: 19652–19664.
- Liang, Z.; Li, Z.; Xu, S.; Tan, M.; and Jia, K. 2021. Instance segmentation in 3D scenes using semantic superpoint tree networks. In *Proceedings of the IEEE International Conference on Computer Vision*, 2783–2792.

- Lin, T.-Y.; Goyal, P.; Girshick, R.; He, K.; and Dollár, P. 2017. Focal loss for dense object detection. In *Proceedings* of the *IEEE international conference on computer vision*, 2980–2988.
- Liu, Y.; Ott, M.; Goyal, N.; Du, J.; Joshi, M.; Chen, D.; Levy, O.; Lewis, M.; Zettlemoyer, L.; and Stoyanov, V. 2019. Roberta: A robustly optimized bert pretraining approach. *arXiv preprint arXiv:1907.11692*.
- Liu, Z.; Zhang, Z.; Cao, Y.; Hu, H.; and Tong, X. 2021. Group-free 3d object detection via transformers. In *Proceedings of the IEEE International Conference on Computer Vision*, 2949–2958.
- Luo, G.; Zhou, Y.; Sun, X.; Cao, L.; Wu, C.; Deng, C.; and Ji, R. 2020. Multi-task collaborative network for joint referring expression comprehension and segmentation. In *Proceedings of the IEEE Conference on computer vision and pattern recognition*, 10034–10043.
- Luo, J.; Fu, J.; Kong, X.; Gao, C.; Ren, H.; Shen, H.; Xia, H.; and Liu, S. 2022. 3d-sps: Single-stage 3d visual grounding via referred point progressive selection. In *Proceedings of the IEEE Conference on Computer Vision and Pattern Recognition*, 16454–16463.
- Milletari, F.; Navab, N.; and Ahmadi, S.-A. 2016. V-net: Fully convolutional neural networks for volumetric medical image segmentation. In 2016 fourth international conference on 3D vision (3DV), 565–571. Ieee.
- Qi, C. R.; Yi, L.; Su, H.; and Guibas, L. J. 2017. Pointnet++: Deep hierarchical feature learning on point sets in a metric space. *Advances in neural information processing systems*, 30.
- Rezatofighi, H.; Tsoi, N.; Gwak, J.; Sadeghian, A.; Reid, I.; and Savarese, S. 2019. Generalized intersection over union: A metric and a loss for bounding box regression. In *Proceedings of the IEEE conference on computer vision and pattern recognition*, 658–666.
- Roh, J.; Desingh, K.; Farhadi, A.; and Fox, D. 2022. Languagerefer: Spatial-language model for 3d visual grounding. In *Conference on Robot Learning*, 1046–1056. PMLR.
- Schult, J.; Engelmann, F.; Hermans, A.; Litany, O.; Tang, S.; and Leibe, B. 2023. Mask3D: Mask Transformer for 3D Semantic Instance Segmentation. In 2023 IEEE International Conference on Robotics and Automation (ICRA), 8216–8223. IEEE.
- Sun, J.; Qing, C.; Tan, J.; and Xu, X. 2023. Superpoint transformer for 3d scene instance segmentation. In *Proceedings of the AAAI Conference on Artificial Intelligence*, volume 37, 2393–2401.
- Wu, Y.; Cheng, X.; Zhang, R.; Cheng, Z.; and Zhang, J. 2023. EDA: Explicit Text-Decoupling and Dense Alignment for 3D Visual Grounding. In *Proceedings of the IEEE Conference on Computer Vision and Pattern Recognition*, 19231–19242.
- Yang, Z.; Zhang, S.; Wang, L.; and Luo, J. 2021. Sat: 2d semantics assisted training for 3d visual grounding. In *Proceedings of the IEEE International Conference on Computer Vision*, 1856–1866.

- Yuan, Z.; Yan, X.; Liao, Y.; Zhang, R.; Wang, S.; Li, Z.; and Cui, S. 2021. Instancerefer: Cooperative holistic understanding for visual grounding on point clouds through instance multi-level contextual referring. In *Proceedings of the IEEE International Conference on Computer Vision*, 1791–1800.
- Zhao, L.; Cai, D.; Sheng, L.; and Xu, D. 2021. 3DVG-Transformer: Relation modeling for visual grounding on point clouds. In *Proceedings of the IEEE International Conference on Computer Vision*, 2928–2937.
- Zhu, C.; Zhou, Y.; Shen, Y.; Luo, G.; Pan, X.; Lin, M.; Chen, C.; Cao, L.; Sun, X.; and Ji, R. 2022. Seqtr: A simple yet universal network for visual grounding. In *European Conference on Computer Vision*, 598–615. Springer.